# Active Antenna Hub: A Multiport Shared-Antenna Architecture for Scalable Internet of Things Devices

Shuyu Wang, *Graduate Student Member, IEEE*, Hanfei Bu, Yongjian Zhang, *Member, IEEE*, Le Chang, *Senior Member, IEEE*, Xi Chen, *Member, IEEE*, Kunpeng Wei, *Senior Member, IEEE*, and Yue Li, *Senior Member, IEEE*

***Abstract*—The Internet of Things (IoT) engineering demands compact, scalable, and multifunctional wireless systems and devices. Conventional wireless architectures rely on multiple and ever-increasing antennas to support new services, leading to increased size, design complexity, and mutual coupling, especially problematic in volume limited terminals. This article presents the "Active Antenna Hub," a novel shared-antenna architecture that enables multiple systems to operate simultaneously using a single electrically small antenna. The proposed architecture integrates a passive antenna, an active matching network based on an ohmic-biased transistor, and Chebyshev bandpass filters for multiband, multiport functionality, supporting wireless system scalability without changes to antennas. To validate, an antenna prototype supporting frequency modulation (FM) and digital television (DTV) services is developed with the system-level experiments, demonstrating the high system scalability and reduced mutual coupling without compromising performance. The proposed Active Antenna Hub architecture offers a compact, scalable, and efficient solution of antennas for next-generation IoT devices.**

***Index Terms*—Active antenna hub, radio frequency (RF) architecture, scalable terminals.**

## I. Introduction

THE Internet of Things (IoT) plays a crucial role in the future of industrial systems and smart living environments by enabling seamless connectivity among smart devices [1], [2], [3], [4], [5]. As wireless communication standards continue to evolve rapidly, IoT devices must frequently undergo hardware upgrades to accommodate emerging systems and new frequency bands, including but not limited to sensors, antennas and radars [6], [7], [8]. Hence, there is a growing demand for hardware platforms that are reusable, flexible, and easily upgradable with minimal physical modifications. To address this need, the concept of the scalable terminal has been introduced [9], [10]. Scalable terminals are built upon radio frequency (RF) architectures that can be dynamically configured to operate across arbitrary frequency bands, providing system expandability for IoT devices. As conceptually illustrated in Fig. 1(a), conventional IoT devices typically employ static RF architectures that use multiple antennas, each assigned to a distinct frequency and wireless standard [11], [12], [13], [14], [15], [16], [17], [18]. Under this architecture, expanding systems requires equipping multiple additional antenna elements with RF circuits. However, this approach is inherently inefficient for subwavelength-sized devices, where limited volume restricts antenna deployment and degrades radiation performance. Furthermore, the close placement of multiple antennas results in strong mutual coupling, which further compromises system efficiency.

To overcome these limitations, significant research has focused on antenna design strategies to support scalable operation. One widely explored solution involves electrically small antennas, which aim to achieve high radiation efficiency within limited volumes [19], [20], [21], [22], [23], [24]. For instance, [19] presents an electrically small antenna for smartwatch applications covering GPS L1, WLAN/Bluetooth, and 5G bands within a $0.22\lambda \times 0.19\lambda$ footprint. Another work [21] proposes a wideband LTE antenna covering 698–960 MHz, 1710–2690 MHz, and 3400–3800 MHz within a compact clearance of $0.12\lambda \times 0.02\lambda$. As an innovative design method, machine learning-based antenna design has also been widely investigated recently [25], [26], [27]. As an example, work [25] utilizes an evolutionary neural network to design a wideband antenna covering 1.7–2.7 GHz. However, the small size of electrically small antennas often restricts their bandwidth and limits their ability to support future system expansions. Another line of research has explored filtering antennas to mitigate interantenna coupling through out-of-band suppression [28], [39]. These designs incorporate filtering functions either directly into the radiating structure or within the feed network. For example, [28] introduces a waveguide-based filtering antenna that operates at 2.49–2.56 GHz and 3.37–3.49 GHz, while [29] presents a dielectric antenna with integrated dielectric strips for operation in

Received 7 August 2025; accepted 17 August 2025. Date of publication 20 August 2025; date of current version 24 October 2025. This work was supported in part by the National Key Research and Development Program of China under Grant 2021YFA0716601, and in part by the National Natural Science Foundation of China under Grant U22B2016. *(Corresponding author: Yue Li.)*

Shuyu Wang, Hanfei Bu, and Yongjian Zhang are with the Department of Electronic Engineering, Tsinghua University, Beijing 100084, China.

Le Chang is with the Shaanxi Key Laboratory of Deep Space Exploration Intelligent Information Technology, and the School of Information and Communications Engineering, Xi'an Jiaotong University, Xi'an 710049, China.

Xi Chen is with the Beijing National Research Center for Information Science and Technology, Tsinghua University, Beijing 100084, China.

Kunpeng Wei is with the the Department of Smartphone, Xiaomi Communications Company Ltd., Beijing 100085, China.

Yue Li is with the Department of Electronic Engineering, the Beijing National Research Center for Information Science and Technology, and the State Key Laboratory of Space Network and Communications, Tsinghua University, Beijing 100084, China (e-mail: lyee@tsinghua.edu.cn).

Digital Object Identifier 10.1109/JIOT.2025.3600758

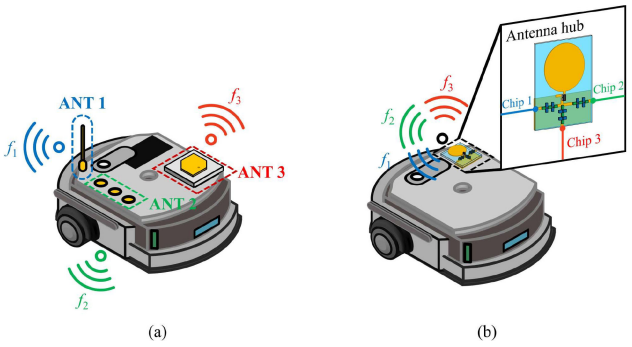


Fig. 1. Application scenario of IoT device with (a) conventional RF architecture, and (b) active antenna hub architecture.

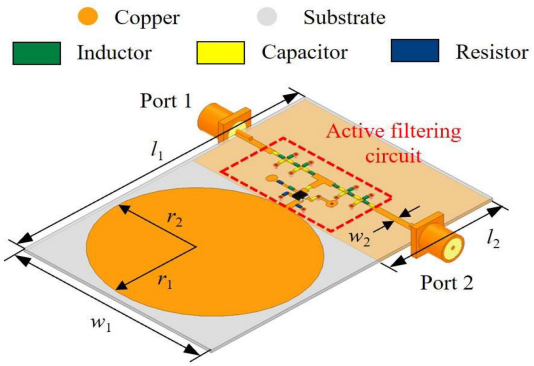


Fig. 2. Geometrical configuration of the active antenna hub.

7.3–8.16 GHz and 13.1–13.6 GHz bands. Similarly, [36] uses a dual-band filtering feedline to excite the antenna at 1.71–2.17 GHz and 3.22–3.7 GHz. Although these filtering antennas improve out-of-band isolation, their fixed frequency responses lack the dynamic configurability necessary for scalable terminals. In summary, current RF architectures and antenna designs are inadequate for scalable terminal requirements, necessitating the development of a novel RF architecture suitable for future IoT devices.

In this article, we propose an innovative architecture termed the "Active Antenna Hub," tailored especially for scalable IoT devices. As depicted in Fig. 1(b), this architecture employs a single electrically small antenna that concurrently supports multiple wireless systems through multiple configurable ports. Each port in the active antenna hub is assigned a customizable frequency window, i.e., operating frequency and bandwidth, to accommodate different communication standards. Unlike conventional architectures, the proposed design enables system expansion without adding new antennas or redesigning the existing one, while maintaining high intersystem isolation within a compact footprint. The active antenna hub is realized by integrating an electrically small passive antenna with an active impedance matching network based on an ohmic-biased transistor (OBT), and a set of parallel Chebyshev lumped-element bandpass filters. The active matching network compensates for impedance mismatches and enables broadband frequency agility. The Chebyshev filters provide sharp out-of-band rejection, effectively minimizing cross-band interference and enhancing signal-to-noise ratio (SNR). To validate the proposed architecture, we designed and fabricated a two-port, dual-band prototype supporting frequency modulation (FM) and digital television (DTV). The prototype achieves operating bands of 74–108 MHz (FM) and 476–764 MHz (DTV), with reflection coefficients below -10 dB and interport isolation exceeding 45 dB. Additionally, the design exhibits steep roll-off characteristics of 121.5 dB/GHz in the FM band and 129.5 dB/GHz in the DTV band. The successful system-level demonstration of simultaneous FM and DTV reception verifies the feasibility of the proposed concept and highlights its promise for future scalable and volume-limited IoT devices.

## II. Antenna Concept and Design

### A. Active Antenna Hub Configuration

The perspective view of the proposed active antenna hub is illustrated in Fig. 2. The active antenna hub is constructed by compactly integrating an OBT circuit and bandpass filters with a small monopole antenna. The monopole antenna is fabricated on an FR-4 epoxy substrate ($\varepsilon_r = 4.4$, $\tan\delta = 0.02$, where $\varepsilon_r$ represents the relative permittivity and $\delta$ represents dielectric loss angle). The substrate thickness is 0.6 mm, with a length of $l_1 = 60$ mm and a width of $w_1 = 40$ mm. The monopole structure consists of an elliptical radiator and a ground plane. The radiator has a major radius of $r_2 = 19.2$ mm and a minor radius of $r_1 = 17.8$ mm, while the ground plane spans the full substrate width with a length of $l_2 = 24.6$ mm. To realize the filtering functionality, the active filtering circuit is implemented on the top side of the substrate, and the ground plane on the bottom side also serves as the circuit ground. The microstrip lines in the active filtering circuit have a width of $w_2 = 1.2$ mm, corresponding to a 50 Ω impedance. As illustrated in Fig. 2, the circuit elements are denoted by color-coded blocks: black for the field-effect transistor (FET) functioning as the OBT, green for inductors, yellow for capacitors, and blue for resistors. Two SMA connectors are mounted on opposite sides of the antenna, serving as output ports to support multisystem operation.

### B. Active Circuit Design

The circuit diagram of the proposed active antenna hub is shown in Fig. 3(a), where color-coded frames represent the various functional modules. The active filtering circuit comprises a cascaded configuration of an OBT matching network and a pair of parallel Chebyshev bandpass filters. To further explain the operating mechanism, an equivalent model of the OBT circuit is illustrated in Fig. 3(b). In this model, the electrically small passive antenna is equivalent to a voltage source with internal capacitance $C_A$, while the OBT is a voltage-controlled current source gm with input and output elements. The transistor gate is equivalent to the input capacitor $C_G$, and $R_D$ represents the channel resistance of the transistor. Additionally, the parasitic capacitor at drain is represented with $C_D$. During operation, $C_A$ and $C_G$ form a capacitance voltage division, converting the electric field coupled by the antenna to the gate voltage. The field effect then transfers the gate voltage to the drain current, enabling power transmission. By biasing the transistor in the ohmic region, the

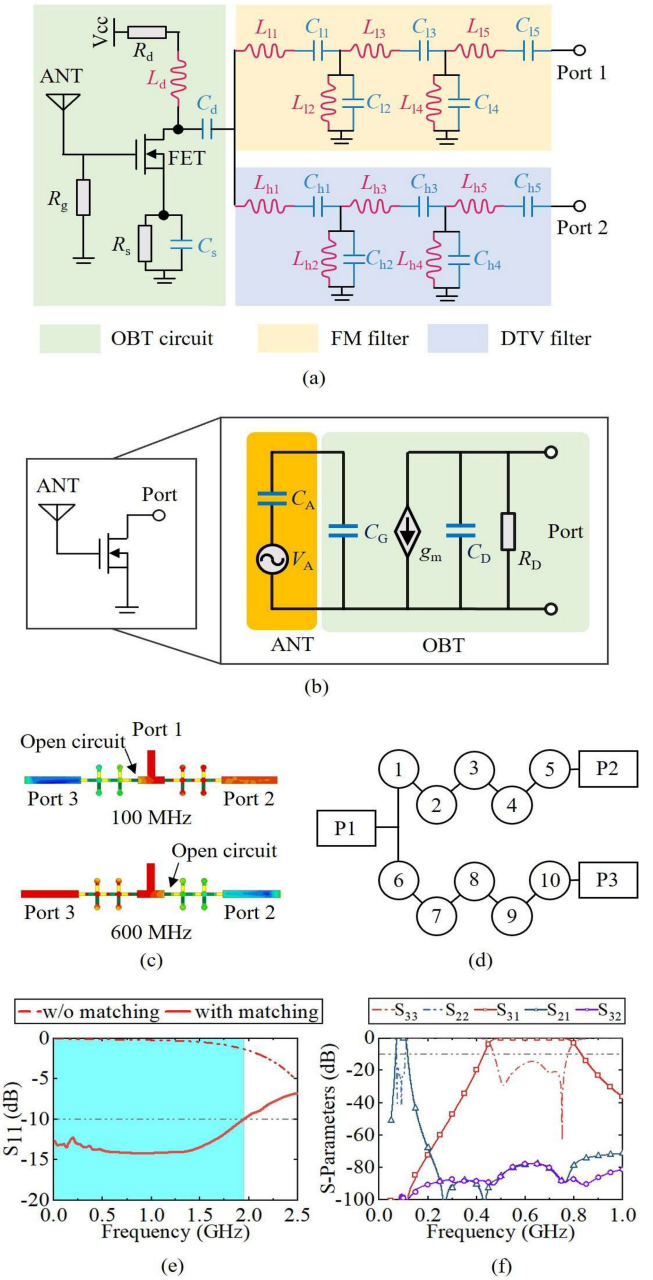


Fig. 3. (a) Circuit diagram of the filtering antenna. (b) Equivalent circuit of the OBT circuit. (c) Current distribution of the paralleled filters at 100 MHz and 600 MHz. (d) Resonator-based topology of the proposed filtering circuit. (e) Simulated reflection coefficient of the antenna with OBT circuit. (f) Simulated *S*-parameters of the paralleled circuits.

drain resistor is configured to be 50 Ω, forming a wideband impedance matching with the port. It is worth mentioning that the parasitic capacitor $C_D$ determines the bandwidth of the OBT antenna. The simulated current distribution at 100 MHz and 600 MHz are depicted in Fig. 3(c), and the corresponding simulated *S*-parameters are provided in Fig. 3(f). As shown, the interfilter isolation exceeds 78 dB within each filter's passband, confirming negligible cross-coupling. The resonator-based topology of the filters is illustrated in Fig. 3(d), while Fig. 3(e) compares the antenna's reflection coefficient with and without the OBT circuit. Without OBT matching, the reflection coefficient is close to 0 dB, indicating poor impedance matching. In contrast, the inclusion of the OBT circuit reduces the reflection coefficient below −10 dB across 10 MHz to 1.8 GHz. Therefore, the achievable tuning range for the antenna is limited to this frequency span by the bandwidth of the OBT circuit. Conventional impedance matching methods employ conjugate matching. However, the impedance of an antenna at electrically small size varies rapidly with the frequency, therefore the matched bandwidth is narrow. Comparing to conventional impedance matching methods, the OBT circuit matching is based on the channel resistance $R_D$ of the transistor, which is stable across the frequency spectrum, and provides a wide bandwidth. Therefore, the OBT circuit provides the Active Antenna Hub with a wide frequency window configuration range, which also supports compact antenna designs. Based on this advancement, the Active Antenna Hub could be utilized to support arbitrary wireless systems in IoT devices. This advancement in the matching methodology is a key enabler for the proposed Active Antenna Hub, allowing it to flexibly accommodate various wireless standards. Such capability is particularly valuable in IoT devices, where compactness, frequency agility, and support for diverse communication protocols are essential.

TABLE I
CIRCUIT ELEMENT VALUES IN FIG. 3(A)

| OBT circuit | | FM filter | | DTV filter | |
|---|---|---|---|---|---|
| Element | Value | Element | Value | Element | Value |
| $R_g$ | 11 kΩ | $L_{l1}$ | 180 nF | $L_{h1}$ | 22 nH |
| $R_d$ | 120 Ω | $L_{l2}$ | 24 nF | $L_{h2}$ | 4.5 nH |
| $R_s$ | 11 Ω | $L_{l3}$ | 390 nF | $L_{h3}$ | 43 nH |
| $L_d$ | 180 nH | $L_{l4}$ | 24 nF | $L_{h4}$ | 4.5 nH |
| $C_d$ | 47 nF | $L_{l5}$ | 180 nF | $L_{h5}$ | 22 nH |
| $C_s$ | 47 nF | $C_{l1}$ | 17 pF | $C_{h1}$ | 3.3 pF |
| Vcc | 2.8 V | $C_{l2}$ | 120 pF | $C_{h2}$ | 11 pF |
| | | $C_{l3}$ | 8 pF | $C_{h3}$ | 1.5 pF |
| | | $C_{l4}$ | 120 pF | $C_{h4}$ | 11 pF |
| | | $C_{l5}$ | 17 pF | $C_{h5}$ | 3.3 pF |

The specific component values used in the circuit are listed in Table I. In the configuration of the proposed Active Antenna Hub, the passive antenna element is connected to the gate of the OBT, and bias resistors $R_g$, $R_d$, and $R_s$ are used for the gate, drain and source, respectively, ensuring operation in the ohmic region. According to the datasheet, the transistor operates in its ohmic region with near 50 Ω drain impedance with bias voltage $V_{GS} = -0.22$ V and $V_{GS} = 0.18$ V, where $I_D = 20$ mA. The gate resistor $R_g = 11$ kΩ is first chosen to ensure that the gate is at 0-V bias. Then, source resistor $R_s$ is calculated as $-V_{GS}/I_D = 10$ Ω. $R_d$ is chosen as 120 Ω. Therefore, the biasing voltage yields $\text{Vcc}=V_{DS}-V_{GS}+I_D \times R_d = 2.8$ V. Choking inductor $L_d = 180$ nH and blocking capacitors $C_s$ and $C_d$ of 4.7 nF isolates the RF signal from the direct current (DC) bias.

As discussed in [42], an electrically small monopole antenna exhibits an impedance that can be expressed as

$$Z_{\text{ANT}} = 80\left(\frac{\pi l}{\lambda}\right)^2 - j \cdot 50 \cot\left(\frac{\pi l}{\lambda}\right) \quad (1)$$

where $l$ is the physical length of the antenna, and $\lambda$ represents the free-space wavelength of the operating frequency. In the context of FM and DTV applications, the antenna length ($l_1 = 60$ mm) is much smaller than the corresponding wavelength ($l \ll \lambda$), resulting in a capacitive input impedance unsuitable for direct reception. To achieve broadband impedance matching, OBT technology is adopted [41], [42], where the antenna is connected to the gate of the FET, and the drain is connected to the output port. The drain impedance of the OBT is derived as [43]

$$Z_{\text{drain}} = \frac{1}{[2K_n(V_{\text{GS}} - V_T - V_{\text{DS}})]} \tag{2}$$

where $K_n$ represents the conduction parameter of the FET; $V_{GS}$ and $V_{DS}$ denote the gate-source and drain-source bias voltages, respectively, and $V_T$ is the FET threshold voltage. By tuning the bias voltages, the impedance can be flexibly matched over a wide frequency range. Notably, (2) is frequency-independent, which supports the frequency- window configurability required by the active antenna hub-based scalable terminals. In Fig. 3(a), the OBT matching network is highlighted in green. In this configuration, the passive antenna element is connected to the gate of the OBT, and bias resistors $R_g$, $R_d$, and $R_s$ are used for the gate, drain and source, respectively, ensuring operation in the ohmic region. Choking inductor $L_d$ and blocking capacitors $C_s$ and $C_d$ isolate the RF signal from the DC bias. It is noticeable that as shown in the circuit diagram, the antenna in its current configuration is that it is receive-only. However, by incorporating technologies, such as reconfigurable antennas, the design's capability could potentially be extended to support transmission as well.

Two Chebyshev bandpass filters operating at the FM and DTV bands are connected in parallel to the drain of the OBT, indicated in yellow and blue in Fig. 3(a). These filters share a common input impedance $Z_{\text{drain}}$ as the OBT and have an output impedance of 50 Ω to match the port. The transfer function of an $n$th order Chebyshev bandpass filter is given by

$$\|H_n(\omega)\|^2 = \frac{1}{1+\varepsilon^2 T_n{}^2\left[\frac{\omega_0}{\omega_2-\omega_1}\left(\frac{\omega}{\omega_0}-\frac{\omega_0}{\omega}\right)\right]} \tag{3}$$

where $\varepsilon$ represents the ripple constant; $Tn$ is the $n$th order Chebyshev function; $\omega_1$, $\omega_2$ and $\omega_0$ represent the lower and upper cut-off frequencies, and passband center frequency, respectively. Using the insertion loss method, filters with arbitrary passbands can be flexibly designed, supporting customizable frequency windows [44], [45]. In this design, a 5th-order Chebyshev filter is selected for its steep roll-off and low-insertion loss. A series-first topology is used so that each filter presents an open-circuit characteristic in its stopband. This ensures minimal cross-talk when filters are paralleled, thereby maintaining high interport isolation. Additionally, since the filters are implemented using lumped inductors and capacitors, their passbands can be dynamically tuned. As demonstrated in [46], varactor diodes and p-i-n diodes can be used to tune capacitive and inductive elements, respectively, enabling reconfigurability of the filtering antenna.

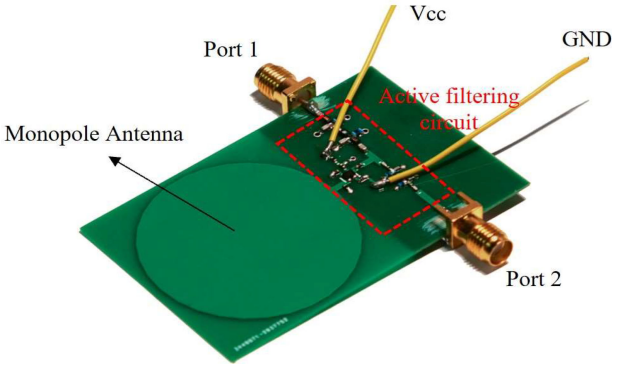


Fig. 4. Application scenario of the active antenna hub: sharing a single antenna by multiple communication systems.

## III. Simulation and Measurement Results

Based on the design analysis, a prototype of the active antenna hub for FM and DTV bands is fabricated. A photograph of the fabricated prototype is shown in Fig. 4. The antenna configuration and circuit design follow the schematic in Fig. 2, where an active filtering circuit is integrated with a printed monopole antenna. The circuit is implemented on the top side of the substrate, with all components soldered in place. A high-electron mobility transistor (HEMT), model NE3509M04, is employed as the OBT in the filtering circuit. Copper wires are used to supply the DC bias voltage to the circuit, and two SMA connectors serve as the signal ports of the active antenna hub. To evaluate the prototype's performance, both electromagnetic and circuit simulations are conducted. The electromagnetic structure is analyzed using full-wave simulation software (HFSS), while circuit-level simulations are performed in Cadence Microwave Office. The monopole antenna is first modeled in HFSS, and its radiation and impedance characteristics are extracted and imported into the circuit simulator for co-simulation with the OBT circuit and filters. Measurements are then carried out to validate the simulation results. During the measurement process, the antenna is biased using a DC voltage source. The $S$-parameters of the active antenna hub are measured with a Keysight N9951B vector network analyzer, and gain and radiation patterns are evaluated in an anechoic chamber. To measure gain, a standard procedure is followed using half-wavelength dipole antennas, each fabricated to resonate at specific test frequencies. The gain $G_d$ of the dipole antenna is first measured in the chamber. A continuous-wave signal is then transmitted by a signal generator through one of the dipole antennas. An identical dipole, connected to a spectrum analyzer, receives the signal, and the received power is recorded as $P_1$. The receiving dipole is then replaced by the active antenna hub, with the position and input power kept unchanged. The received power at the active antenna hub is recorded as $P_2$. The realized gain of the proposed antenna is calculated using the relation $G = G_d + P_2 - P_1$.

The noise figure of the OBT matching circuit is measured and presented in Fig. 5. The maximum noise figure of the OBT circuit is 2.08 dB across the operating bandwidth. It is important to note that the noise figure is higher than that of

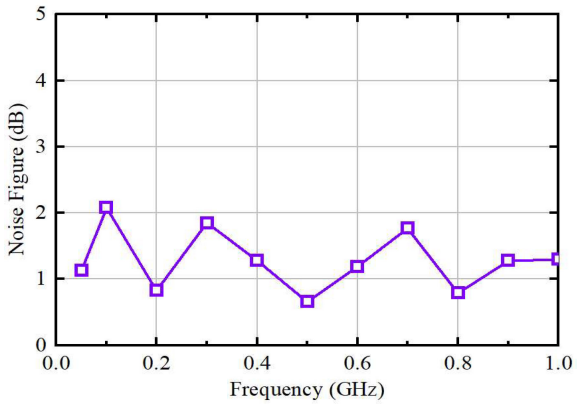


Fig. 5. Measured noise figure of the OBT matching circuit.

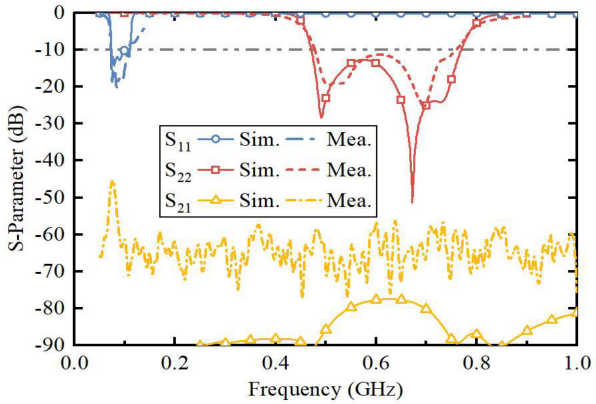


Fig. 6. Simulation and measurement results of the *S*-parameters of the active antenna hub.

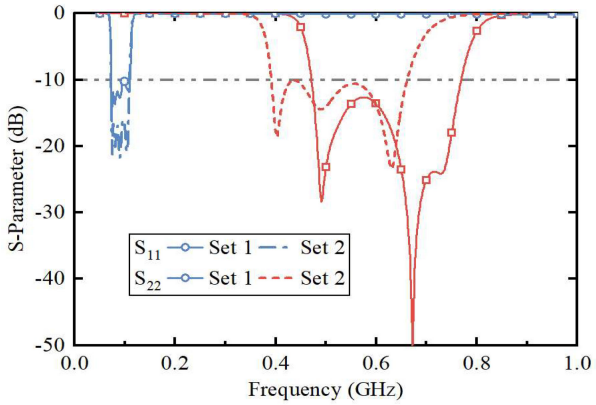


Fig. 7. Simulated reflection coefficients of the two ports with different sets of filter values.

a typical low-noise amplifier (LNA) due to the ohmic-region operation. However, the signal-to-noise degradation introduced by the OBT circuit remains acceptable.

The simulated and measured *S*-parameters of the proposed active antenna hub are shown in Fig. 6. As indicated by the solid lines, the simulated $S_{11}$ of the active antenna hub is below $-10$ dB from 73 MHz to 110 MHz in the pass band, while it approaches 0 dB in the stopband, demonstrating a clear filtering response. Similarly, the simulated $S_{22}$ is below $-10$ dB from 471 MHz to 769 MHz in the passband. The measured $S_11$ and $S_22$ are represented by the dashed lines. Port 1 has a bandwidth from 74 MHz to 108 MHz, while port 2 spans from 476 MHz to 764 MHz. The measured results are in well agreement with the simulations. Notably, $S_{21}$ remains lower than $-45$ dB and is approximately $-60$ dB across the frequency spectrum. This high cross-band isolation is achieved by the paralleled bandpass filters. To demonstrate the tunability of the frequency window, we used two sets of element values for the DTV filter and ran simulations on the antenna (Set 1: $L_{h1} = L_{h5} = 22$ nH, $L_{h2} = L_{h4} = 4.5$ nH, $L_{h3} = 43$ nH, $C_{h1} = C_{h5}$=3.3 pF, $C_{h2} = C_{h4} = 11$ pF, $C_{h3} = 1.5$ pF; Set 2: $L_{h1} = L_{h5} = 15$ nH, $L_{h2} = L_{h4} = 5.5$ nH, $L_{h3} = 40$ nH, $C_{h1} = C_{h5} = 5$ pF, $C_{h2} = C_{h4} = 12$ pF, $C_{h3} = 2.2$ pF). As illustrated in Fig. 7, altering the element values in the DTV filter modifies the frequency window of port 2, while having minimal effect on the reflection coefficient of port 1. The simulation results confirm that the frequency window of the proposed antenna can be independently tuned.

The simulation and measurement results of the active antenna hub gain are depicted in Fig. 8. The measurement results display significant out-of-band suppression with a rapid roll-off. At the FM band, port 1 of the proposed active antenna hub exhibits a receiving gain of $-19.2$ dBi, with a roll-off rate of 2340 dB/GHz at the lower edge and 1215 dB/GHz at the upper edge. An out-of-band suppression of 60 dB is observed, confirming its filtering response. Port 2, operating in the DTV band, achieves a gain of 0.2 dBi, with roll-off rates of 388 dB/GHz at the lower edge and 244 dB/GHz at the upper edge. The out-of-band suppression for port 2 exceeds 80 dB. The measurement results validate that the active antenna hub possesses a rapid roll-off and superior frequency-selective behavior. The coupling between ports is minimal, ensuring highly effective suppression of cross-band interference. Based on the simulation and measurement results, it is indeed true that the antenna gain is lower in the FM band compared to the DTV band. The primary reason for this gain reduction is that at lower frequencies, the antenna has a smaller electrical size. As a result, more electromagnetic waves resonate in the near-field of the antenna, which are then deteriorated due to the substrate loss (FR-4 epoxy). To mitigate this gain decay, a feasible solution would be to use a low-loss substrate, such as Teflon or Rogers.

The 3-D and 2-D radiation patterns are illustrated in Fig. 9. Fig. 9(a) and (b) represent the simulated and measured radiation patterns for port 1 at 80 MHz and 100 MHz, respectively, while Fig. 9(c) and (d) showcase the radiation patterns at 500 MHz and 700 MHz fed from port 2. As observed, the radiation patterns demonstrate a donut-shape, characteristic of a small monopole antenna.

To highlight the merits of the proposed active antenna hub, a performance comparison between this work and state-of-the-art dual-band filtering antennas is presented in Table II. In the table, $\lambda_{LL}$ represents the wavelength at the lower frequency edge of the lower band, and $\lambda_{HH}$ represents the wavelength at the upper frequency edge of the upper band. Among the designs, References [28], [29], [30], and [38] realize structure filtering

TABLE II
PERFORMANCE COMPARISON OF MULTIBAND FILTERING ANTENNAS

| Reference | Bandwidths (%) | Volume ($\lambda_{LL}^3$) | Frequency ratio ($\lambda_{HH}/\lambda_{LL}$) | Out-of-band Suppression (dB) | Lower band roll-off rate (dB/GHz) | Upper band roll-off-rate (dB/GHz) |
|---|---|---|---|---|---|---|
| **[36]** | 4.2 / 3.8 | 0.7×0.7×0.03 | 1.51 | 25 / 18 | 88.4 / 123.7 | 41.25 / 70.7 |
| **[35]** | 12.3 / 7.6 | 0.71×0.71×0.12 | 1.58 | > 17.7 | 29.6 / 26.3 | 101.4 / 26.6 |
| **[28]** | 2.7 / 3.3 | 1.05×1.03×0.02 | 1.4 | 38 / 28.6 | 131.7 / 237 | 79 / 237 |
| **[29]** | 11.4 / 4.8 | 7.3×7.3×0.66 | 1.86 | > 15 | 11.3 / 32.7 | 18.6 / 36.5 |
| **[30]** | 7.7 / 14 | 0.34×0.34×0.13 | 1.52 | > 17 | N.A. / 79.4 | 112.5 / N.A. |
| **[34]** | 23.7 / 13.9 | 0.24×0.24×0.18 | 2.16 | 20 / 30 | 35.8 / 43.4 | 21.2 / 58.3 |
| **[38]** | 3.1 / 9.2 | 0.41×0.28×0.05 | 1.5 | >13 | 167 / 71.4 | 167 / 41.7 |
| **[39]** | 24 / 11.76 | 0.66×0.66×0.27 | 1.6 | 10 | 45.5 / 61.8 | 77.2 / 96.6 |
| **This work** | **37 / 46.4** | **0.014×0.009×0.00015** | **10.3** | **60 / 80** | **2340 / 1215** | **388 / 244** |

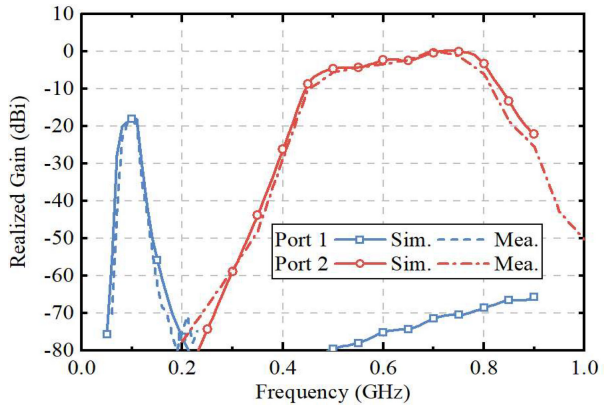


Fig. 8. Simulation and measurement results of the realized gain of the active antenna hub.

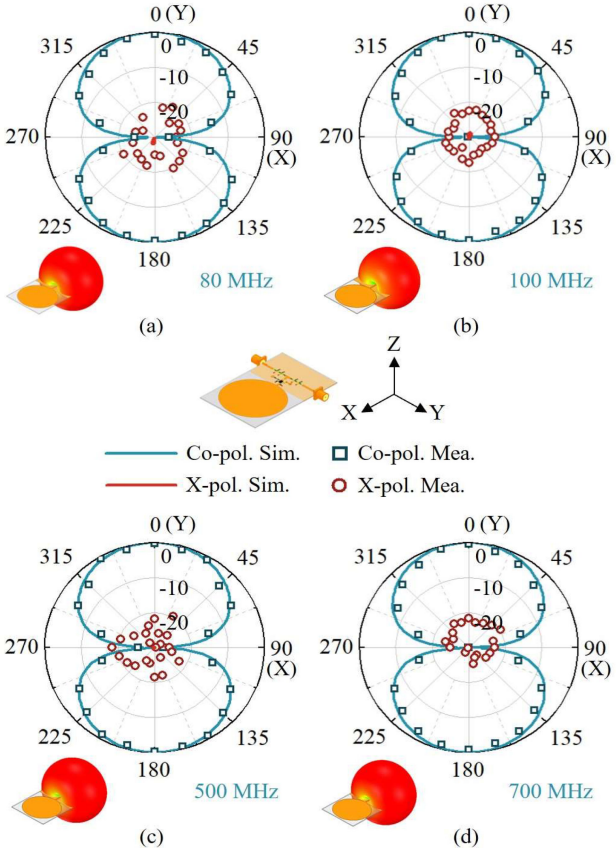


Fig. 9. Simulated and measured radiation patterns of the active antenna hub at (a) 80 MHz, (b) 100 MHz, (c) 500 MHz, and (d) 700 MHz.

antennas, while References [34], [35], [36], and [39] implement feed filtering antennas. It is noticeable that the frequency ratio of the previously proposed dual-band antennas is limited to approximately 2, which does not meet the requirements of diverse system applications. In contrast, benefiting from the active filtering circuit based on OBT impedance matching, the active antenna hub proposed in this work achieves a much larger frequency ratio of 10.3, revealing its flexibility of configuration and expansion. Additionally, owing to the small antenna impedance matching capability of the OBT circuit, the active antenna hub exhibits a significantly miniaturized volume. The inclusion of 5th order Chebyshev filters in the active filtering circuit ensures that the active antenna hub provides superior out-of-band suppression and roll-off rates compared to other filtering antennas reported in the literature.

To provide a comprehensive perspective of the Active Antenna Hub against conventional filtering antennas, the pros and cons are listed in a bulleted format as the followings.

*1) Conventional Filtering Antennas [28], [29], [30], [31], [32], [33], [34], [35], [36], [37], [38], [39]:*

*Pros:* high efficiency, no DC power consume.

*Cons:* lack of configurability, limited dual-band frequency ratio, narrow bandwidth, relatively large physical size.

*2) Proposed Active Antenna Hub:*

*Pros:* frequency window configurability, wide bandwidth, electrically small size.

*Cons:* reduced efficiency due to circuit element loss, consumes DC power.

It is notable that a single wideband antenna can cover the desired bandwidth. However, directly connecting a wideband antenna to multiple systems can lead to severe mutual coupling between the systems, resulting in performance degradation. In contrast, as illustrated in Fig. 5 of the manuscript, the dual-band filtering antenna not only provides out-of-band suppression for the systems but also achieves high port isolation.

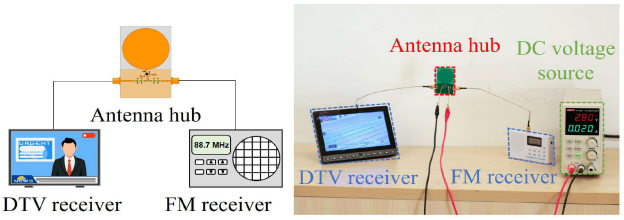


Fig. 10. Demo system of the active antenna hub. (a) Schematic of the demo system by sharing the active antenna hub with a DTV receiver and an FM receiver. (b) Photograph of the demo system.

## IV. Discussion

### A. System Demonstration

To validate the performance of the active antenna hub in real-life scenarios, a system demonstration for simultaneous FM and DTV signal reception is conducted. The schematic of the system setup is illustrated in Fig. 10(a). Port 1 of the active antenna hub is connected to an FM receiver, while port 2 is connected to a DTV receiver. In this demonstration, the active antenna hub receives the broadcasting FM and DTV signals from the air, and the receivers decode and play the video and audio, respectively. Fig. 10(b) presents the photograph of the system in operation. The FM receiver successfully demodulates the signal at 92.0 MHz, while the DTV receiver receives the signal at 516 MHz. A video of the demonstration is provided in the Supplementary Video. Utilizing the active antenna hub, the video and audio outputs from the receivers are clear and smooth, without noticeable noise or disruptions. This system demonstration confirms that the active antenna hub functions effectively in real-life scenarios, thereby validating its practical application performance.

### B. 3-Port Active Antenna Hub Extension

The framework of designing active antenna hub can be extended to accommodate additional frequency windows by adding paralleled bandpass filters in the active filtering circuit. To demonstrate this flexibility, a 3-port active antenna hub is designed for receiving FM, DTV and global navigation satellite system (GNSS) signals. The active antenna hub configuration is shown in Fig. 11(a). The antenna element is identical to that used in the 2-port active antenna hub. A 3-port active filtering circuit is integrated with the monopole antenna, providing three output ports for FM, DTV and GNSS signals, respectively. Fig. 11(b) illustrates the circuit diagram of the 3-port active antenna hub. In addition to the active filtering circuit in the 2-port active antenna hub, an additional 5th order Chebyshev filter for GNSS reception, is paralleled with the FM and DTV filters. The circuit element values for the GNSS filter, including $L_{g1}$ to $L_{g5}$ and $C_{g1}$ to $C_{g5}$, are listed in Table III, with the remaining element values unchanged from those in Table I.

The simulated $S$-parameters of the 3-port active antenna hub are illustrated in Fig. 12(a). The $S_{11}$ and $S_{22}$ of the active antenna hub are lower than -10 dB in the 73–110 MHz and 471–769 MHz bands, respectively, consistent with the

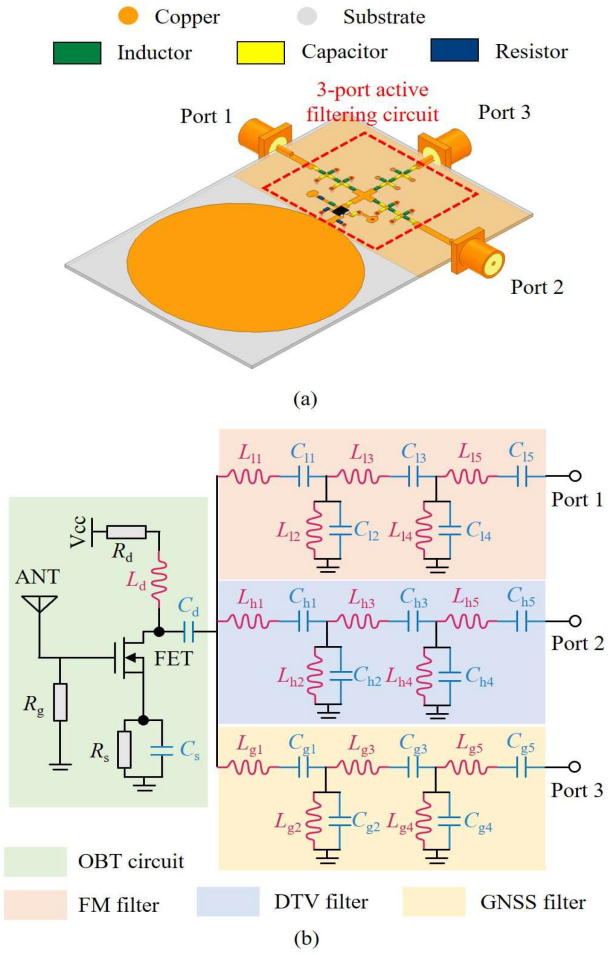


Fig. 11. (a) Schematic of the 3-port active antenna hub operating at FM, DTV and GNSS bands, respectively. (b) Circuit diagram of the 3-port active antenna hub.

TABLE III
Circuit Element Values in Fig. 11(b)

| OBT circuit | | FM filter | | DTV filter | | GNSS filter | |
|---|---|---|---|---|---|---|---|
| Element | Value | Element | Value | Element | Value | Element | Value |
| $R_g$ | 11 kΩ | $L_{l1}$ | 180 nF | $L_{h1}$ | 22 nH | $L_{g1}$ | 7.32 nH |
| $R_d$ | 120 Ω | $L_{l2}$ | 24 nF | $L_{h2}$ | 4.5 nH | $L_{g2}$ | 0.97 nH |
| $R_s$ | 11 Ω | $L_{l3}$ | 390 nF | $L_{h3}$ | 43 nH | $L_{g3}$ | 20.26 nH |
| $L_d$ | 180 nH | $L_{l4}$ | 24 nF | $L_{h4}$ | 4.5 nH | $L_{g4}$ | 0.97 nH |
| $C_d$ | 47 nF | $L_{l5}$ | 180 nF | $L_{h5}$ | 22 nH | $L_{g5}$ | 7.32 nH |
| $C_s$ | 47 nF | $C_{l1}$ | 17 pF | $C_{h1}$ | 3.3 pF | $C_{g1}$ | 1.56 pF |
| Vcc | 2.8 V | $C_{l2}$ | 120 pF | $C_{h2}$ | 11 pF | $C_{g2}$ | 4.3 pF |
| | | $C_{l3}$ | 8 pF | $C_{h3}$ | 1.5 pF | $C_{g3}$ | 0.53 pF |
| | | $C_{l4}$ | 120 pF | $C_{h4}$ | 11 pF | $C_{g4}$ | 4.3 pF |
| | | $C_{l5}$ | 17 pF | $C_{h5}$ | 3.3 pF | $C_{g5}$ | 1.56 pF |

performance of the 2-port active antenna hub. $S_{33}$ is lower than −10 dB from 1.15 GHz to 1.64 GHz, covering the required GNSS band. The isolation between the ports exceeds 50 dB. The simulation results of the receiving gain are depicted in Fig. 12(b). All 3 ports exhibit highly effective frequency filtering responses with rapid roll-off. At the GNSS band, the gain reaches 4.34 dBi, with a roll-off of 144 dB/GHz at the lower edge and 108.5 dB/GHz at the upper edge.

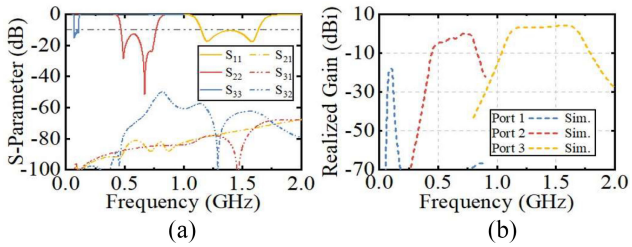


Fig. 12. Simulation results of the (a) *S*-parameters and (b) realized gain.

The results confirm that the 3-port active antenna hub effectively supports the reception of FM, DTV and GNSS signals. Furthermore, all characteristics of the active antenna hub can be customized to meet specific requirements. The number of frequency windows is determined by selecting the number of filters in the filtering circuit. The width and center frequency of each frequency window can be independently configured by adjusting the values of the filter elements. By increasing the orders of the Chebyshev filters in the circuit, the roll-off performance can be further enhanced. Additionally, as discussed in [41] and [42], the frequency window distribution range can be expanded by selecting a FET with a narrower gate width, while the overall gain of the active antenna hub can be increased by enlarging the passive antenna element. Through this approach, an active antenna hub with arbitrarily distributed frequency windows and adjustable receiving gain is achieved. The novelty of the proposed Active Antenna Hub lies in its shared-antenna architecture, which enables both bandwidth and center frequency configurability without requiring significant hardware modifications. This flexible design supports compatibility with multiple wireless standards and systems, making it highly adaptable for scalable IoT deployments. Additionally, the antenna maintains an electrically compact form factor, allowing seamless integration into terminals of various sizes and shapes. These features, combined with its wide bandwidth and tunable frequency range, position the Active Antenna Hub as a strong candidate for next-generation IoT devices requiring dynamic, multiband operation in space-constrained environments.

## V. Conclusion

This article introduced the "Active Antenna Hub," a scalable, compact RF front-end architecture for IoT devices. By integrating a passive electrically small antenna with an OBT impedance matching circuit and parallel bandpass filters, the design enables broadband matching, effective out-of-band suppression, and high-intersystem isolation. Unlike conventional multiantenna systems, the Active Antenna Hub allows multiple wireless systems to operate concurrently through a shared, electrically small antenna, promoting hardware reuse and easier adaptation to new frequency bands. To validate the proposed concept, a dual-band prototype supporting FM and DTV systems was designed, fabricated, and tested. System-level experiments, including simultaneous FM and DTV signal reception, confirm the feasibility and effectiveness of the architecture. Furthermore, we discuss the extensibility of the design, demonstrating its potential to support additional ports and frequency windows with ease. With its compactness, flexibility, and scalability, the Active Antenna Hub is well-suited for emerging IoT applications across smart cities [47], industrial automation [48], consumer electronics [19], and connected healthcare [49]. This work establishes a foundation for further research and commercialization of shared-antenna solutions in the IoT domain.

## References

[1] H. Tran-Dang, N. Krommenacker, P. Charpentier, and D.-S. Kim, "Toward the Internet of Things for physical Internet: Perspectives and challenges," *IEEE Internet Things J.*, vol. 7, no. 6, pp. 4711–4736, Jun. 2020.

[2] T. B. da Silva, R. P. dos Santos Chaib, C. S. Arismar, R. da Rosa Righi, and A. M. Alberti, "Toward future Internet of Things experimentation and evaluation," *IEEE Internet Things J.*, vol. 9, no. 11, pp. 8469–8484, Jun. 2022.

[3] A. M. Alberti, G. D. Scarpioni, V. J. Magalhães, A. Cerqueira, J. J. P. C. Rodrigues, and R. da Rosa Righi, "Advancing novagenesis architecture towards future Internet of Things," *IEEE Internet Things J.*, vol. 6, no. 1, pp. 215–229, Feb. 2019.

[4] Y. Wang, L. Sun, Z. Du, and Z. Zhang, "Antenna design for modern mobile phones: A review," *Electromag. Sci.*, vol. 2, no. 2, 2024, Art. no. 60521.

[5] M. M. Islam, S. Nooruddin, F. Karray, and G. Muhammad, "Internet of Things: Device capabilities, architectures, protocols, and smart applications in healthcare domain," *IEEE Internet Things J.*, vol. 10, no. 4, pp. 3611–3641, Feb. 2023.

[6] Q. Li, S. Liao, Y. Yang, Z. Liang, and S. Xiao, "Wideband 5G millimeter-wave MIMO magnetoelectric dipole antenna integrated with partially reflective surfaces," *IEEE Trans. Antennas Propag.*, vol. 72, no. 1, pp. 445–453, Jan. 2024.

[7] M. Hajizadegan, M. Sakhdari, S. Liao, and P.-Y. Chen, "High-sensitivity wireless displacement sensing enabled by PT-symmetric telemetry," *IEEE Trans. Antennas Propag.*, vol. 67, no. 5, pp. 3445–3449, May 2019.

[8] L. Zhu, N. Alkhaldi, H. M. Kadry, S. Liao, and P.-Y. Chen, "A compact hybrid-fed microstrip antenna for harmonics-based radar and sensor systems," *IEEE Antennas Wireless Propag. Lett.*, vol. 17, no. 12, pp. 2444–2448, Dec. 2018.

[9] A. Mavromatis, A. P. Da Silva, K. Kondepu, D. Gkounis, R. Nejabati, and D. Simeonidou, "A software defined device provisioning framework facilitating scalability in Internet of Things," in *Proc. IEEE 5G World Forum (5GWF)*, Silicon Valley, CA, USA, 2018, pp. 446–451.

[10] T. N. Gia, A. -M. Rahmani, T. Westerlund, P. Liljeberg, and H. Tenhunen, "Fault tolerant and scalable IoT-based architecture for health monitoring," in *Proc. IEEE Sens. Appl. Symp. (SAS)*, Zadar, Croatia, 2015, pp. 1–6.

[11] Y. Zhang, Y. Li, W. Wang, Z. Zhang, and Z. Feng, "Omnidirectional antenna diversity system for high-speed onboard communication," *Engineering*, vol. 11, pp. 72–79, Apr. 2022.

[12] Y. Zhang and Y. Li, "Wideband microstrip antenna in small volume without using fundamental mode," *Electromag. Sci.*, vol. 1, no. 2, pp. 1–6, Jun. 2023.

[13] Z. Zhou et al., "The low-attenuation endfire leaky-wave state on an optically transparent lossy film," *Engineering*, vol. 43, pp. 72–80, Dec. 2024.

[14] H. Li, Z. Zhou, Y. Zhao, and Y. Li, "Low-loss beam synthesizing network based on Epsilon-near-zero (ENZ) medium for on-chip antenna array," *Chip*, vol. 2, no. 2, Jun. 2023, Art. no. 100049.

[15] C. Zhang, S. Liao, and M. Li, "Scattering matrix based IMPM for multiport antenna systems," *IEEE Antennas Wireless Propag. Lett.*, vol. 24, pp. 2562–2566, 2025.

[16] Y. Zhang, "Differential antennas: Fundamentals and applications," *Electromag. Sci.*, vol. 1, no. 1, 2023, Art. no. 10021.

[17] W. Qiu, J. Li, P. Xiao, and S. Liao, "A novel metasurface-based decoupler for wideband stacked patch antenna array," in *Proc. IEEE 22nd Int. Conf. Commun. Technol. (ICCT)*, Nanjing, China, 2022, pp. 717–721.

[18] A. Askarian and K. Wu, "Aperture-shared radiation surface: A promising technique for multifunctional antenna array development," *Electromag. Sci.*, vol. 1, no. 3, 2023, Art. no. 30082.

[19] B. Xiao, H. Wong, D. Wu, and K. L. Yeung, "Design of small multiband full-screen smartwatch antenna for IoT applications," *IEEE Internet Things J.*, vol. 8, no. 24, pp. 17724–17733, Dec. 2021.
[20] H. Liu, S. Gao, and T. -H. Loh, "Small director array for low-profile smart antennas achieving higher gain," *IEEE Trans. Antennas Propag.*, vol. 61, no. 1, pp. 162–168, Jan. 2013.
[21] K.-L. Wong and Y.-C. Chen, "Small-size hybrid loop/open-slot antenna for the LTE smartphone," *IEEE Trans. Antennas Propag.*, vol. 63, no. 12, pp. 5837–5841, Dec. 2015.
[22] C. Zhu et al., "Electrically small metamaterial-inspired tri-band antenna with meta-mode," *IEEE Antennas Wireless Propag. Lett.*, vol. 14, pp. 1738–1741, 2015.
[23] X. Yang, Y. Z. Yin, W. Hu, and S. L. Zuo, "Low-profile, small circularly polarized inverted-L antenna with double-folded arms," *IEEE Antennas Wireless Propag. Lett.*, vol. 9, pp. 767–770, 2010.
[24] S. Tu, Y.-C. Jiao, Z. Zhang, Y. Song, and S.-M. Ning, "Small internal 2.4-GHz/UWB antenna for wireless dongle applications," *IEEE Antennas Wireless Propag. Lett.*, vol. 9, pp. 284–287, 2010.
[25] J. Li et al., "An adaptive evolutionary neural network-based optimization design method for wideband dual-polarized antennas," *IEEE Trans. Antennas Propag.*, vol. 71, no. 10, pp. 8165–8172, Oct. 2023.
[26] S. Liao and L. Ou, "The ping-pong electromagnetic algorithm for reflecting surface antennas of arbitrary shapes," *IEEE Trans. Antennas Propag.*, vol. 70, no. 4, pp. 2855–2862, Apr. 2022.
[27] S. Liao and R. J. Vernon, "A fast algorithm for computation of electromagnetic wave propagation in half-space," *IEEE Trans. Antennas Propag.*, vol. 57, no. 7, pp. 2068–2075, Jul. 2009.
[28] L. Li, S. X. Wu, D. Pang, X. Zhang, and Q. Wang, "A fifth-order single-layer dual-band half-mode SIW filtering antenna with a multifunctional single slot," *Antennas Wireless Propag. Lett.*, vol. 20, no. 9, pp. 1676–1680, Sep. 2021.
[29] K. Xu, L. Jin, H. Tang, W.-W. Yang, and J. Shi, "A high-efficiency dual-band self-filtering antenna based on three dense dielectric strip resonators," *IEEE Antennas Wireless Propag. Lett.*, vol. 21, pp. 1532–1536, 2022.
[30] S. J. Yang, W. Duan, Y. Y. Liu, H. Ye, H. Yang, and X. Y. Zhang, "Compact dual-band base-station antenna using filtering elements," *IEEE Trans. Antennas Propag.*, vol. 70, no. 8, pp. 7106–7111, Aug. 2022.
[31] C. F. Ding, Z. -Y. Zhang, Y. Zeng, and M. Yu, "Dual-band dual-polarized base-station antenna design using filtering dipole elements," *IEEE Trans. Antennas Propag.*, vol. 71, no. 2, pp. 1931–1936, Feb. 2023.
[32] N. An and Y. Zhang, "Dual-band dual-sense circularly polarized antenna utilizing a radiating slot antenna as feeding structure," *IEEE Antennas Wireless Propag. Lett.*, vol. 23, pp. 1321–1325, 2024.
[33] P. F. Hu, Y. M. Pan, X. Y. Zhang, and S. Y. Zheng, "A compact filtering dielectric resonator antenna with wide bandwidth and high gain," *IEEE Trans. Antennas Propag.*, vol. 64, no. 8, pp. 3645–3651, Aug. 2016.
[34] J. Li, J. Li, J. Yin, C. Guo, H. Zhai, and Z. Zhao, "A miniaturized dual-band dual-polarized base station antenna loaded with duplex baluns," *IEEE Antennas Wireless Propag. Lett.*, vol. 22, pp. 1756–1760, 2023.
[35] Y. Li, Z. Zhao, Z. Tang, and Y. Yin, "Differentially fed, dual-band dual-polarized filtering antenna with high selectivity for 5G sub-6 GHz base station applications," *IEEE Trans. Antennas Propag.*, vol. 68, no. 4, pp. 3231–3236, Apr. 2020.
[36] C. X. Mao et al., "Dual-band patch antenna with filtering performance and harmonic suppression," *IEEE Trans. Antennas Propag.*, vol. 64, no. 9, pp. 4074–4077, Sep. 2016.
[37] J. Li, S. Wu, Y. Li, X. Chen, S. Yan, and X. Y. Zhang, "SLA printed dual-band conical-beam filtering antenna," *IEEE Antennas Wireless Propag. Lett.*, vol. 22, pp. 2462–2466, 2023.
[38] J. Shi, Y. He, and H. Sun, "Compact dual-band filtering microstrip antenna using spoof surface plasmon polaritons feed line," *IEEE Antennas Wireless Propag. Lett.*, vol. 24, pp. 127–131, 2025.
[39] H. Yuan, F.-C. Chen, and K.-R. Xiang, "A sub-6 GHz dual-band dual-polarized filtering antenna," *IEEE Antennas Wireless Propag. Lett.*, vol. 24, pp. 908–912, 2025.
[40] C. A. Balanis, *Antenna Theory—Analysis and Design*, 4th ed. New York, NY, USA: Wiley, 2016, ch. 4.
[41] S. Wang and Y. Li, "Single-transistor impedance matching circuit for over-hundred-octave active antennas," *IEEE Trans. Antennas Propag.*, vol. 72, no. 3, pp. 2391–2398, Mar. 2024.
[42] S. Wang, Z. Liu, Y. Zhang, and Y. Li, "Active-passive reconfigurable antenna covering 70-7200 MHz bandwidth," *IEEE Trans. Antennas Propag.*, vol. 72. no. 9, pp. 7323–7328, Sep. 2024.
[43] D. A. Neamen, *Semiconductor Physics and Devices: Basic Principles*. 4th ed. New York, NY, USA: McGraw Hill, 2012.
[44] D. M. Pozar, *Microwave Engineering*, 4th ed. New York, NY, USA: Wiley, 2011.
[45] A. Li et al., "Innovative inverse-design approach for on-chip computational spectrometers: Enhanced performance and reliability," *Engineering*, vol. 43, pp. 81–88, Dec. 2024.
[46] Y. Li, Z. Zhang, Z. Feng, and M. F. Iskander, "A beam steerable CPW-CTS antenna array using reconfigurable metamaterial-based phase shifters for cognitive radio applications," in *Proc. URSI General Assembly Sci. Symp. (URSI GASS)*, Beijing, China, 2014, pp. 1–4.
[47] E. H. Houssein, M. A. Othman, W. M. Mohamed, and M. Younan, "Internet of things in smart cities: Comprehensive review, open issues, and challenges," *IEEE Internet Things J.*, vol. 11, no. 21, pp. 34941–34952, Nov. 2024.
[48] V. Graveto, T. Cruz, and P. Simões, "Using KNX-based building automation and control systems for data exfiltration," *IEEE Internet Things J.*, vol. 10, no. 15, pp. 13727–13741, Aug. 2023.
[49] S. Liu, Y. Huang, A. Kong, J. Tang, and X. Liu, "Rise of the automotive health-domain controllers: Empowering healthcare services in intelligent vehicles," *IEEE Internet Things J.*, vol. 9, no. 24, pp. 24882–24889, Dec. 2022.

**Shuyu Wang** (Graduate Student Member, IEEE) received the B.S. degree in electronic engineering from Tsinghua University, Beijing, China, in 2022, where he is currently pursuing the Ph.D. degree in electronic engineering.

His current research interests include electrically small antennas, active circuits, and wideband active antennas.

Mr. Wang serves as a reviewer for IEEE TRANSACTIONS ON ANTENNAS AND PROPAGATION and *Microwave and Optical Technology Letters*.

**Hanfei Bu** received the B.S. degree in electronic engineering from Tsinghua University, Beijing, China, in 2025, where he is currently pursuing the Ph.D. degree in electronic engineering.

His current research interests include electrically small antennas and metamaterials.

**Yongjian Zhang** (Member, IEEE) received the B.S. degree in communication engineering from Tongji University, Shanghai, China, in 2018, and the Ph.D. degree in electronic engineering from Tsinghua University, Beijing, China, in 2023.

He is currently a Postdoctoral Fellow with the Department of Electronic Engineering, Tsinghua University. His current research interests include aircraft antennas, dual-polarized antennas, and multiple-input and multiple-output antenna arrays.

Dr. Zhang serves as a reviewer for IEEE TRANSACTIONS ON ANTENNAS AND PROPAGATION, IEEE ANTENNAS AND WIRELESS PROPAGATION LETTERS, and *Microwave and Optical Technology Letters*.

**Le Chang** (Senior Member, IEEE) received the B.S. degree in electronics and information engineering from Xidian University, Xi'an, China, in 2012, and the Ph.D. degree in electrical engineering from Tsinghua University, Beijing, China, in 2017.

In July 2017, he joined Huawei Technology Ltd., Beijing, China, as a Senior Antenna Engineer. Since 2021, he has been with Xi'an Jiaotong University, Xi'an, where he is currently an Associate Professor. He has authored or co-authored 45 journal articles. His current research interests include mobile antennas and mmW/THz antennas.

**Xi Chen** (Member, IEEE) received the B.S. degree in telecommunication engineering from Beijing University of Posts and Telecommunications, Beijing, China, in 2001, and the Ph.D. degree from Tsinghua University, Beijing, China, in 2006.

He is currently with Beijing National Research Center for Information Science and Technology, Tsinghua University, as an Associate Professor. His research interests include synergy of satellite communication and navigation, and massive signals of opportunity positioning.

**Kunpeng Wei** (Senior Member, IEEE) received the B.S. degree in electronic and information engineering from Huazhong University of Science and Technology, Wuhan, China, in 2008, and the Ph.D. degree in electrical engineering from Tsinghua University, Beijing, China, in 2013.

In 2012, he was a Visiting Scholar with the School of Electrical and Computer Engineering, Georgia Institute of Technology, Atlanta, GA, USA. From July 2013 to December 2015, he was employed with the Radar Research Institute, Chinese Air Force Research Laboratory, Beijing, conducting research in the areas of phased-array antenna design and radar system design. He joined Consume Business Group of Huawei Inc., Shenzhen, China, in 2016, where he had been an Antenna Specialist and the Director of Xi'an Antenna Team. Since 2021, He joined Honor Device Company Ltd., Shenzhen, when this company split from Huawei and he was the Director of Honor Antenna Team. After leaving Honor, he joined Xiaomi Corporation, Beijing, in 2023. He is currently the Chief Antenna Expert and the Head of the Antenna Technology Team. He is also an Adjunct Professor with School of Electronics and information engineering, Shenzhen University, Shenzhen. He leads a large group of antenna experts and engineers and takes the full responsibility in the research of antenna technologies to guarantee the market success of all Xiaomi's products ranging from smartphones, electric cars, tablets and other IoT devices. He has authored over referred 60 papers on consumer electronics antenna design. He holds over 100 granted U.S./EU/JP/CN patents and has other 20+ patent applications in pending. His current research interests include MIMO antenna technology, satellite communication technology, 5.5G/millimeter wave technology, UWB wireless technology and meta-antennas for Human × Car × Home smart ecosystem.

Dr. Wei was a recipient of the Principal Scholarship of Tsinghua University in 2012, the Huawei Individual Gold Medal Award in 2018, the Huawei Team Gold Medal Award in 2017, and the Honor Team Gold Medal Awad in 2021, respectively. He is serving as an Associate Editor for *IET Electronics Letters* since October 2021 and IEEE OPEN JOURNAL OF ANTENNAS AND PROPAGATION since October 2023. He is also a special level external expert of the China Academy of Information and Communications Technology. He is an IET Fellow.

**Yue Li** (Senior Member, IEEE) received the B.S. degree in telecommunication engineering from Zhejiang University, Zhejiang, China, in 2007, and the Ph.D. degree in electronic engineering from Tsinghua University, Beijing, China, in 2012.

In June 2012, he was a Postdoctoral Fellow with the Department of Electronic Engineering, Tsinghua University. In December 2013, he was a Research Scholar with the Department of Electrical and Systems Engineering, University of Pennsylvania, Philadelphia, PA, USA. He was also a Visiting Scholar with the Institute for Infocomm Research, A*STAR, Singapore, in 2010, and Hawaii Center of Advanced Communication, University of Hawaii at Manoa, Honolulu, HI, USA, in 2012. Since January 2016, he has been with Tsinghua University, where he is currently an Assistant Professor. He is an Associate Professor with the Department of Electronic Engineering, Tsinghua University. He has authored and co-authored over 260 journal articles and 50 international conference papers and holds 25 granted Chinese patents. His current research interests include metamaterials, plasmonics, electromagnetics, nanocircuits, mobile and handset antennas, MIMO and diversity antennas, and millimeter-wave antennas and arrays.

Dr. Li was a recipient of the Issac Koga Gold Medal from the URSI General Assembly. He served as an Associate Editor for IEEE TRANSACTIONS ON ANTENNAS AND PROPAGATION and IEEE ANTENNAS AND WIRELESS PROPAGATION LETTERS from 2017 to 2024. He is also serving as an Associate Editor for *Microwave and Optical Technology Letters* and *Computer Applications in Engineering Education*.